NANO LETTERS

Letter

pubs.acs.org/NanoLett

Uniform and Ordered Copper Nanomeshes by Microsphere Lithography for Transparent Electrodes

Tongchuan Gao,[†] Baomin Wang,[†] Bo Ding,[‡] Jung-kun Lee,[‡] and Paul W. Leu*[,†]

[†]Department of Industrial Engineering and [‡]Department of Mechanical Engineering and Materials Science, University of Pittsburgh, Pittsburgh, 15261

Supporting Information

ABSTRACT: We report a comprehensive simulation and experimental study on the optical and electronic properties of uniform and ordered copper nanomeshes (Cu NMs) to determine their performance for transparent conductors. Our study includes simulations to determine the role of propagating modes in transmission and experiments that demonstrate a scalable, facile microsphere-based method to fabricate NMs on rigid quartz and flexible polyethylene terephthalate substrates. The fabrication method allows for precise control over NM morphology with near-perfect uniformity and long-range order over large areas on rigid substrates. Our Cu NMs demonstrate 80% diffuse transmission at 17 Ω/square on quartz, which is comparable to indium tin oxide. We also performed durability experiments that demonstrate these Cu NMs are robust from bending, heating, and abrasion.

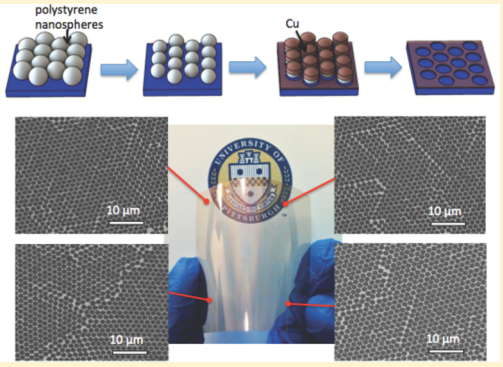

KEYWORDS: *Self-assembly, transparent conductors, flexible optoelectronics, microsphere lithography*

Transparent conductors are important as the top electrode for a variety of optoelectronic devices, including solar cells, flat panel displays, touch screens, and light-emitting diodes. Currently, indium tin oxide (ITO) films are the most commonly used transparent conductor,[1] but indium (In) is a rare earth metal with rising cost.[2] ITO is commercially deposited by costly dc-magnetron sputtering and involves high temperatures making it unsuitable for organic devices.[3] ITO is also brittle, making it unsuitable for emerging flexible electronics as well as resistive touch screens. To decrease manufacturing costs and improve the performance on flexible devices, a variety of nanostructured materials have emerged as potential substitutes for doped metal oxides, such as random carbon nanotube networks[4−7] and graphene.[8,9] However, carbon-based transparent conductors are limited by high sheet resistance.[10] Random silver (Ag) nanowire films fabricated by solution-based methods have demonstrated superior optical transmission and sheet resistance compared to ITO films.[11−13] However, the abundance of Ag in the Earth's crust is comparable to that of In, and the price of Ag and In have been about the same over the past several years.

In contrast, copper (Cu) is far more abundant than In and Ag, and its price is about 2 orders of magnitude lower.[14] Printable random Cu nanowire networks have shown impressive optoelectronic properties comparable to ITO.[15−17] However, random Cu nanowire networks have several fabrication and performance disadvantages. The synthesis of printable metal nanowire solutions requires sophisticated solution processing to obtain high aspect ratio nanowires.[12] Distinct chemistries must be utilized for synthesizing different metals. Percolation may also be a serious problem in these random structures. The density of the nanowires must be above the percolation threshold to form a connected current pathway.[18] However, to achieve high transparency, the networks should be sparse, resulting in poor connectivity and high resistivity such that some nanomaterials are unusable for transparent electrodes. This is especially a problem at the contacts between nanowires, where there is high contact resistance, and for Cu, which has a tendency to oxidize. As reported, random nanowire networks have been shown to fail from ohmic heating in short times.[19] The growth of long wires,[13] mechanical pressing,[13] plasmonic welding,[20] and surface passivation[17] have been alternatively proposed as a means to reduce junction resistance. Recently, electrospun nanotroughs have been reported with transparencies of about 90% at 2 Ω/square[21] and random Au nanomeshes (NMs) prepared by grain boundary lithography have demonstrated 82.5% transmission at about 20 Ω/square.[22] However, these structures, like random nanowire networks, lack uniformity and ordering.

The ability to carefully control morphology with high uniformity and ordering are beneficial for many transparent conductor optoelectronic applications but approaches such as electron beam lithography[23] are not scalable. Nanoimprint lithography has been demonstrated for fabricating metal gratings with high resolution and high throughput.[24] However,

Received: January 24, 2014
Revised: February 28, 2014
Published: March 6, 2014

scalability is a challenge for this methodology since large contact areas between the mold and the imprinted nanostructures can result in sticking issues and pattern fidelity is poor over large areas since the polymer chains in the materials tend to elastically relax.[25] The nanoimprint mold must be patterned by unscalable methods such as electron beam lithography or focused ion beam, and the mold tends to wear with usage. Nanoimprint lithography is also unsuitable for directly fabricating nanostructures on flexible substrates due to the high pressure and temperatures required. While transfer printing methods have been adapted for these purposes,[26] it would nevertheless be advantageous to directly fabricate the transparent electrode onto the device. These imprinted Cu structures also have not performed as well as ITO as discussed below in Figure 1.

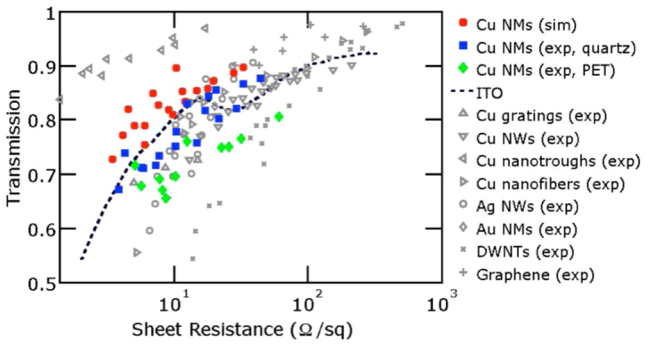

Figure 1. Transmission versus sheet resistance for various transparent conductors. Our Cu nanomesh (NM) data is shown for simulations (red circles) and experimentally on quartz (blue squares) and PET (green diamonds) substrates at λ = 550 nm. The best data that the authors are aware of for ITO thin films,[12] periodically perforated Cu gratings,[24] Cu NWs,[16] electrospun Cu nanotroughs,[21] electrospun Cu nanofibers,[29] Ag NWs,[12] random Au NMs by boundary lithography,[22] double walled carbon nanotubes (DWNTs),[30] and graphene[9] are also shown.

In this paper, we report both a simulation and experimental investigation of Cu NMs as transparent conducting electrodes. The Cu NM consists of holes arranged in a hexagonal lattice in a Cu thin film. We perform electrodynamic simulations and transport simulations to show that Cu NMs may achieve higher optical transmission than ITO films at the same sheet resistance. We also demonstrate a low-cost approach for fabricating metal NMs by microsphere lithography, which is a fast and scalable method compatible with well-established wafer-scale photolithography processes.[27,28] NMs may be fabricated over large areas with precise control over morphology and with high uniformity and order. The as-prepared transparent conductors should have a more uniform resistance and optical properties on the microscale compared with random networks of nanowires. The NMs also have less hazy appearance due to reduced light scattering. Our methodology is versatile in that it may be used to fabricate NMs of any metal that may be deposited through standard evaporation processes. Metal NMs may be fabricated on both rigid or flexible substrates and the morphology may be carefully controlled for various plasmonic applications such as optical filters or sensors, or the formation of ohmic or Schottky barrier contacts for different optoelectronic devices. We demonstrate the fabrication of Cu NMs directly on both rigid quartz and flexible PET substrates and determine that they have comparable performance to ITO films when fabricated on quartz and slightly poorer performance on PET. In addition, we performed durability experiments to assess the performance of Cu NMs under various bending, heating, and abrasion conditions.

Figure 1 plots the relationship between transmission and sheet resistance for a variety of transparent conductors. Our simulation data for Cu NMs is plot with red circles, and our experimental data on quartz and PET substrates is plot with blue squares and green diamonds respectively. Our transmission data is plot at the wavelength λ = 550 nm, which is near the middle of the visible spectrum. The effect of the substrates has been excluded. For comparison purposes, we plot simulation data for ITO thin films,[12] as well as the best experimental data in the literature for several alternative transparent conductors: electrospun Cu nanotroughs[21] and nanofibers,[29] nanoimprinted Cu gratings,[24] solution-coated random Cu NW networks,[16] solution-processed random Ag NW networks,[12] random Au NMs by boundary lithography,[22] dip-coated solution-processed double walled carbon nanotubes (DWNT) films,[30] and roll-to-roll synthesized and transferred graphene.[9] The data shown for the random Ag NW networks[12] is the weighted average of the spectral transmission with the AM1.5 global photon flux over the wavelength range λ = 400 to 800 nm, and the data for the nanimprinted Cu gratings[24] is the average transmittance over the wavelength range λ = 400 to 800 nm. The rest of the data are shown for λ = 550 nm. Our simulation data predicts that Cu NMs may be more transmissive than ITO films for the same sheet resistance. Our experimental data demonstrates that Cu NMs fabricated on quartz substrates exhibit comparable performance to ITO films. More details about the simulations and experiments and differences in the results between the two will be discussed later in the text.

Figure 2 shows our simulation results. Figure 2a shows the schematic for the Cu NMs studied in simulations. The Cu NMs consist of a Cu thin film with holes in a hexagonal array. The primitive lattice vectors are $\vec{a}_1 = (a,0)$ and $\vec{a}_2 = (a/2,(\sqrt{3}/2)a)$ with $|\vec{a}_1| = |\vec{a}_2| = a$ and $\varphi = 60°$. The morphology of Cu NMs are defined by the thickness of the Cu t, the pitch of the hexagonal array a, and the minimum width of the metal w between holes. The NM width is $w = a - d$, where d is the diameter of the holes. The transmission and sheet resistance of metal nanomeshes is anisotropic but invariant under 60° rotational transformations. We used finite difference time domain simulations to obtain the transmission spectra and finite element method simulations to determine the sheet resistances of these structures. The optical simulations utilized the refractive index for Cu from ref 31 and the transport simulations assumed the Cu resistivity in the NMs is the bulk resistivity ($\rho_{Cu} = 1.68 \times 10^{-8}$ Ω·m). Please see the Supporting Information for details.

For comparing different structures, we utilized the angle-averaged transmission $T = 1/2(T_{xx} + T_{yy})$ and angle-averaged sheet resistance $R_s = 1/2(R_{s,xx} + R_{s,yy})$ where T_{xx} and T_{yy} are the transmission for light polarized in the x- and y-directions respectively, and $R_{s,xx}$ and $R_{s,yy}$ are the sheet resistances in the x- and y-direction. NMs exhibit a 6-fold symmetry and our simulations indicated very little dependence of transmission on polarization and sheet resistance on transport direction. Figure 2b shows a contour plot of the optical transmission for Cu NMs as a function of w between 50 and 120 nm and wavelength between 400 and 1000 nm. The pitch a = 1300 nm

dx.doi.org/10.1021/nl5003075 | Nano Lett. 2014, 14, 2105−2110

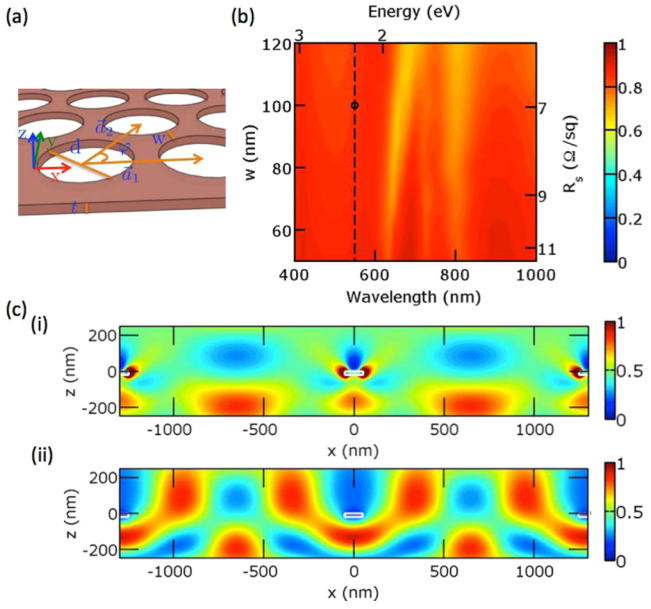

Figure 2. Simulation results. (a) Schematic of Cu NMs simulated, where the morphology consists of a hexagonal array of holes in a metal thin film, where a is the pitch, t is the thickness, and w is the metal width. (b) Contour plot of angle averaged transmission for various w with a = 1300 nm and t = 20 nm as a function of wavelength. The calculated sheet resistance, which depends on w, is shown on the right axis of the plot. The dashed black line indicates λ = 550 nm, which was used in Figure 1. (c) Electric field intensity $|E|^2$ at λ = 550 mn for incident light polarized in the (i) x- and (ii) y-direction for w = 100 nm, which is indicated by the black circle in (b). The edges of the NM cross section are indicated with white lines.

and the thickness t = 20 nm. The simulated angle averaged sheet resistances are shown on the right y-axis. The angle averaged sheet resistances range from R_s = 6.0 Ω/sq for w = 120 nm to R_s = 11.5 Ω/sq for w = 50 nm.

While other work has demonstrated extraordinary transmission for subwavelength holes at particular wavelengths due to surface plasmon modes[32] and propagating plasmonic modesm,[33] the NMs in this work contain apertures with sizes greater than the wavelengths of interest, such that there is broadband transmission close to unity. The transmission spectra is primarily due to the excitation of propagating modes in the NM holes. Cylindrical holes in a perfect metal support propagating modes at wavelengths $\lambda \lesssim 2$,[32] which covers the entire spectrum studied, because the smallest hole diameter studied was d = 1180 nm where w = 120 nm. A broadband transmission over 80% is achievable for $R_s \leq 10$ Ω/sq. In addition, surface waves are resonantly excited by the NMs when $\vec{k}_{spp}(\lambda_{mn}) = \vec{k}_{in,x} + m\vec{b}_1 + n\vec{b}_2$ where $\vec{k}_{spp} = (2\pi/\lambda)[\varepsilon/(\varepsilon + 1)]^{1/2}$ is the wave vector of the surface plasmon polariton, $\vec{k}_{in,x}$ is the in-plane component of the incident wave vector, ε is the permittivity of the Cu, and m and n are integers. The reciprocal lattice basis vectors are $\vec{b}_1 = [(2\pi)/a], -[(2\sqrt{3}\pi)/(3a)]$ and $\vec{b}_2 = (0, [(4\sqrt{3}\pi)/3a]$. For normal incidence light, surface plasmon polaritons are excited when $|\vec{k}_{spp}(\lambda_{mn})| = (2\pi/a)[4/3(m^2 + n^2 - mn)]^{1/2}$. The lowered transparency at 650 nm is due to Fano interference between the two transmission pathways of propagating modes and the (2,1), (1,2), or (1,−1) surface plasmon polariton at λ = 670 nm.[34]

The dashed black line indicates the wavelength λ = 550 nm where the transmission was plotted in Figure 1. Figure 2c shows the electric field intensity at λ = 550 nm in the x−z plane passing though the center of the hole for a NM with a = 1300 nm, w = 100 nm, and t = 20 nm (indicated in Figure 2b with a black circle). The electric field intensity is shown for both light polarized in the (i) x-direction and the (ii) y-direction. The electromagnetic field pattern demonstrates the propagating mode in the holes between the metal, which leads to high transmission. The diameter of the holes d = 1200 nm is much larger than the wavelength λ = 550 nm such that the transmission is close to 100%. The transmission T_{xx} = 84.8% and T_{yy} = 84.9%, while the sheet resistance $R_{s,xx} = R_{s,yy}$ = 7.0 Ω/sq. The transmission of the NM is higher than the geometric aperture, which is $[2\pi(d/2)^2]/(\sqrt{3}a^2)$ = 77.3%. The loss at this wavelength is primarily due to absorption of the metal.

To demonstrate the potential of Cu NMs as a transparent electrode, we developed a large-area, low-cost method to fabricate Cu NMs directly on both rigid quartz and flexible PET substrates. Figure 3a shows a schematic of the microsphere lithography approach for fabricating Cu NMs. The microsphere lithography approach was adapted from nanosphere lithography methods that combine an air/water interface self-assembly technique with a solvent-vapor-annealing method.[35−37] Close-packed hexagonal polystyrene (PS) microspheres were obtained at the air/water interface in a 4″ Petri dish using a self-assembly technique. The area of well-patterned PS microspheres can be scaled up by increasing the size of the container for industrial scale manufacturing. Wire-wound rod coating methods may also be adaptable for this purpose.[38] The patterned microspheres were then transferred to solid substrates dried in air at room temperature. Reactive ion etching (RIE) with oxygen was used to reduce the diameter of the PS microspheres. Cu was then deposited directly onto the PS microsphere patterned substrate with an evaporator at pressures of about 10^{-8} Torr. Finally, the PS microspheres were lifted off by ultrasonication to form Cu NMs. No chemical process was involved in the metal-coating step, thus reducing the cost of reactant. Please refer to Supporting Information for details. This fabrication process may be easily modified for other evaporated metals depending on the particular application. Specific control over metal pitch a, thickness t, and width w may be accomplished through the self-assembly of different diameter microspheres or nanospheres,[37] different etching times, and different evaporation times. Figure 3b shows representative scanning electron microscope (SEM) images of a Cu NM with a = 1300 nm, w = 150 nm, and t = 40 nm fabricated on a rigid quartz substrate. The high uniformity and long-range order of the NM is apparent in the images, where these qualities address the percolation and contact resistance issues of random nanowire networks or disordered structures. Figure 3c shows an optical image of a Cu NM on a flexible PET substrate about 40 cm^2. The figure also shows SEM images of the Cu NM at four different locations, where the NM exhibits more nonuniformities and defects in the lattice on the PET substrate compared to quartz. This is because the assembled microsphere monolayer has more lattice dislocations and defects due to deformation of the PET substrate during self-assembly from its low elasticity. The transparent conductor looks uniform and clear without the appearance of Moiré fringes.

The optical transmittance of the Cu NMs was measured using an integrating sphere. Samples with various morphologies involving different w and t were fabricated and the diffuse transmission at λ = 550 nm was plotted as a function of sheet resistance in Figure 1. The NMs on rigid quartz exhibit higher

dx.doi.org/10.1021/nl5003075 | Nano Lett. 2014, 14, 2105−2110

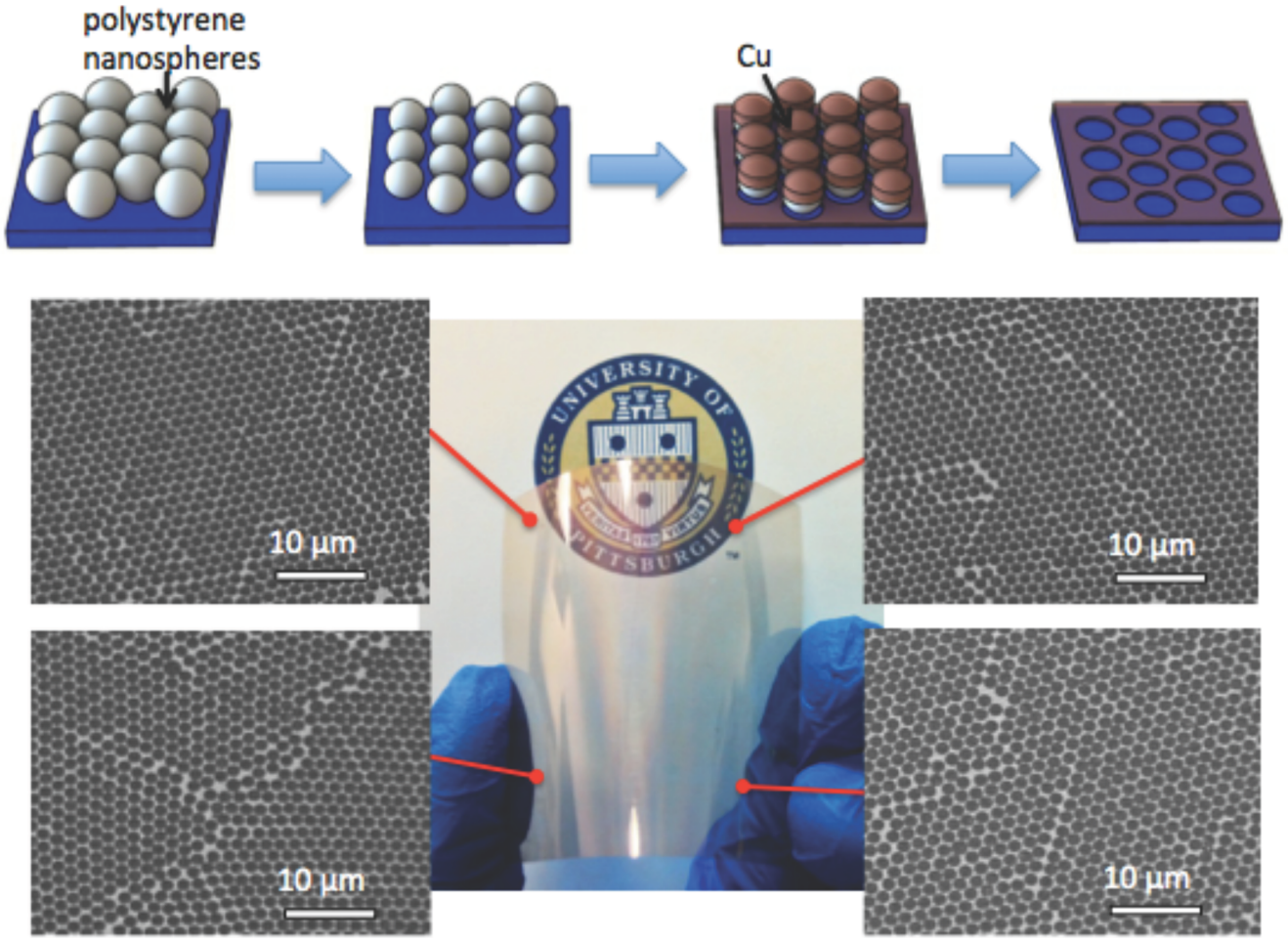

Figure 3. (a) Schematic of the Cu NM fabrication process. (b) SEM images of fabricated Cu NM with a = 1300 nm, w = 150 nm, and t = 40 nm on a rigid substrate. (c) Optical image of a Cu NM fabricated directly on a flexible polyethylene terephthalate (PET) substrate. SEM images show the Cu NM at four various locations.

transmission at a particular sheet resistance than the NMs on the PET substrates due to the better uniformity and ordering of the microspheres during self-assembly. The NMs on quartz achieve 80% transmission with a sheet resistance of 17 Ω/sq, which is comparable to ITO thin films. On PET, the NMs achieve 80% transmission with a sheet resistance of 60.5 Ω/sq and their performance is generally worse than that on quartz.

Figure 4a plots both the simulated and experimentally measured (on quartz) diffuse transmission spectrum for a Cu NM with a = 1300 nm, w = 70 nm, and t = 15 nm. The simulation results represent an averaged result for x- and y-polarized incident light as discussed before. The simulated and experimentally transmission spectra are fairly close to each other, where the slight differences can be accounted for by statistical variations and imperfections in the fabricated structure. The averaged simulated sheet resistance for this NM is 12.1 Ω/sq with $R_{s,xx}$ = $R_{s,yy}$ = 12.1 Ω/sq, while the measured sheet resistance was 20.6 Ω/sq. The NM simulations do not consider surface or grain boundary scattering and thus predict lower sheet resistances than those measured.

Figure 4b shows the simulated diffuse transmission, specular transmission, and absorption versus sheet resistance for Cu NMs with different sheet resistance. The specular transmission was determined from the fraction of power transmitted into the (0,0) diffraction mode and the diffuse transmission was determined from the total transmitted power. See the Supporting Information for details. The average difference between the simulated diffuse and specular transmission is about 2% and the difference increases for samples with larger sheet resistance. Figure 4c shows the experimentally measured diffuse transmission, specular transmission, and absorption versus sheet resistance for various Cu NMs on quartz . For Cu NMs on quartz substrates, the average difference between diffuse and specular transmission is about 4%, which is lower than random Ag NW films which have a difference of about 10%.[13] Less scattering makes the electrode appear less hazy and should be advantageous for applications such as displays. By comparing Figure 4b,c, we notice that simulations overestimate the transmission since the fabricated samples are not perfectly ideal, and the simulated sheet resistance are also lower than the experimental values because bulk resistivity was assumed, which does not consider electron scattering from the grain boundaries and surfaces.

Figure 5 shows the results of various durability tests to evaluate the robustness of the Cu NMs. Figure 5a shows the variation in the sheet resistance of two Cu NMs on PET substrates after both bending in compression and tension. The Cu NM for both bending tests has a geometry of t = 20 nm, a = 1300 nm, and w = 100 nm. The original sheet resistance of the samples prepared for the tension and compression tests are 22.5 and 21.4 Ω/sq respectively. After 150 cycles of bending, the sheet resistance for the samples are 27.2 Ω/sq and 22.6 Ω/

dx.doi.org/10.1021/nl5003075 | Nano Lett. 2014, 14, 2105−2110

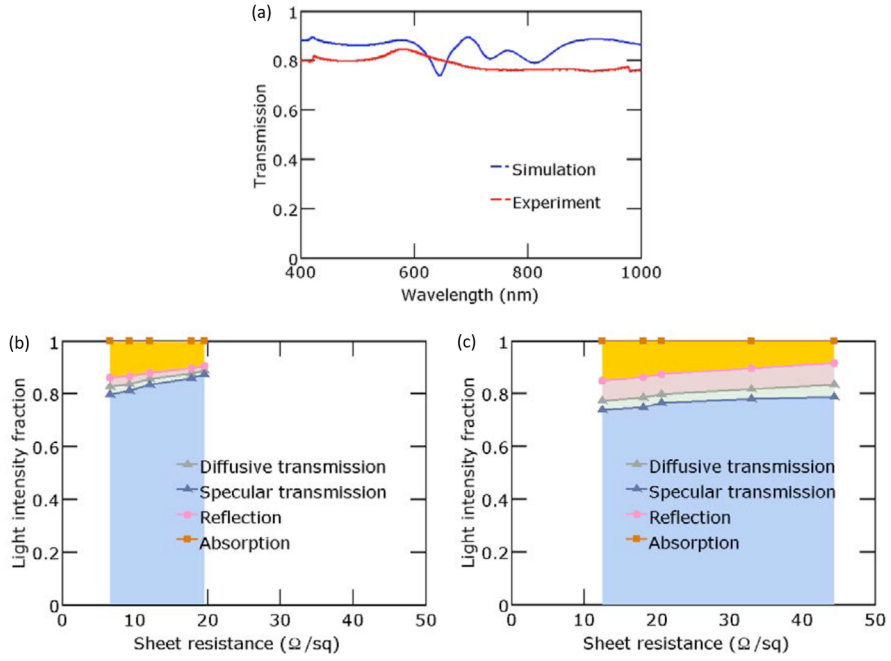

Figure 4. (a) Transmission spectrum for Cu NM with a = 1300 nm, w = 70 nm, and t = 15 nm obtained by simulation and experiment. (b) Plot of simulated diffuse transmission, specular transmission, reflection, and absorption versus sheet resistance for Cu NMs with various geometry at λ = 550 nm. (c) Plot of experimental diffuse transmission, specular transmission, reflection, and absorption versus sheet resistance for a variety of Cu NMs on quartz at λ = 550 nm.

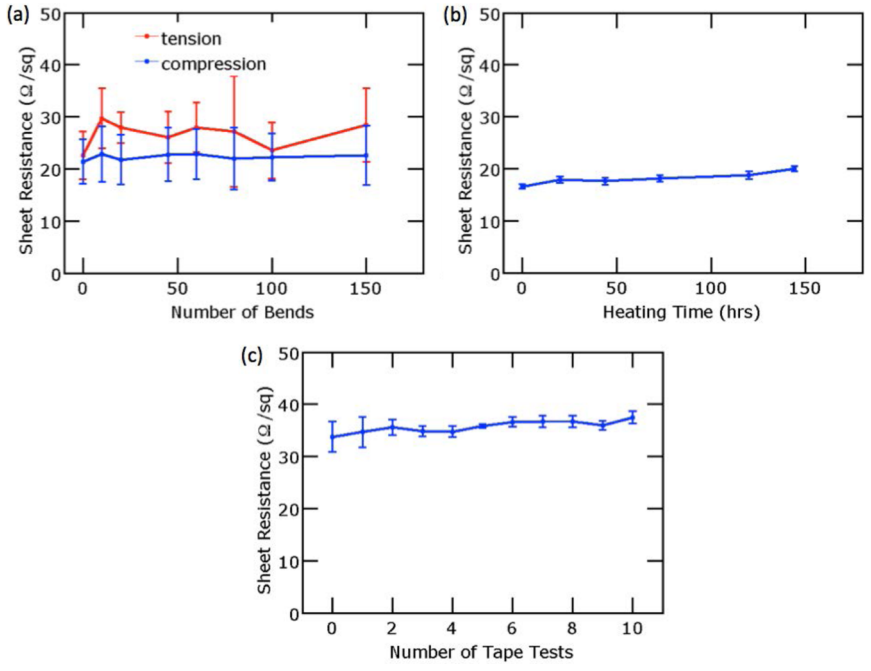

Figure 5. Durability tests for Cu NM on PET substrate. (a) Sheet resistance versus number of bends for Cu NM on PET. The bending curvature is 0.5 in.. (b) Sheet resistance versus heating time for Cu NM heated at 65 °C in air. (c) Sheet resistance versus number of tape tests for Cu NM on PET substrate. Error bars correspond to the standard deviation of four measurements.

sq, demonstrating good durability under bending. Figure 5b shows the change in sheet resistance of a Cu NM on quartz substrates after the heating test. The geometry of the Cu NM is t = 15 nm, a = 1300 nm, and w = 120 nm. The sheet resistance of the sample changed from 16.6 to 20.0 Ω/sq after six days of continuous heating on a hot plate at 65 °C. Cu in particular is prone to oxidation and alloying or passivation of the sample may help reduce sheet resistance degradation, especially at higher temperatures.[39] Figure 5c shows the results of tape tests where Scotch tape was pressed onto the NMs with finger pressure and then pulled off to assess the attachment of the Cu NM to the PET substrate. The geometry of the Cu NM is t = 15 nm, a = 1300 nm, and w = 120 nm. The sheet resistance of the sample only rose from 34.4 to 34.8 Ω/sq after 10 cycles of tape tests.

dx.doi.org/10.1021/nl5003075 | *Nano Lett.* 2014, 14, 2105−2110

In conclusion, we reported both simulations and experiments of Cu NMs. We investigated their transparency and sheet resistance and evaluated the potential of these structures as transparent conductors. Simulated Cu NMs demonstrate the role of propagating modes in transmission and transport simulations compare reasonably to experimental results. We demonstrate a scalable method to fabricate Cu NMs on both rigid quartz substrates and flexible PET substrates. The samples on quartz substrates demonstrate good uniformity and order with performance comparable to ITO, while the PET substrates have slightly poorer performance due to disorder and defects in the NM lattice. Durability tests demonstrate that the NMs are not affected significantly to bending, heating, and abrasion. Future studies may focus on larger pitches, which should offer better transparencies at a given sheet resistance.[40,41] The morphology of these NMs may also be varied for narrowband transmission or filtering for other optoelectronic applications.

■ ASSOCIATED CONTENT

Supporting Information

Methods for optical transmission simulation, sheet resistance simulation, fabrication of Cu NMs, and durability tests. This material is available free of charge via the Internet at http://pubs.acs.org.

■ AUTHOR INFORMATION

Corresponding Author

*E-mail: pleu@pitt.edu.

Notes

The authors declare no competing financial interest.

■ ACKNOWLEDGMENTS

This work was supported in part by NSF Grant 1233151. Computing resources were provided by the Center for Simulation and Modeling at the University of Pittsburgh. The authors would also like to thank the Mascaro Center for Sustainable Innovation for support.

■ REFERENCES

(1) Granqvist, C. G.; Hultåker, A. *Thin Solid Films* **2002**, *411*, 1−5.
(2) Minami, T. *Thin Solid Films* **2008**, *516*, 5822−5828.
(3) Lewis, B. G.; Paine, D. C. *MRS Bull.* **2000**, *25*, 22−27.
(4) Barnes, T. M.; Wu, X.; Zhou, J.; Duda, A.; van de Lagemaat, J.; Coutts, T. J.; Weeks, C. L.; Britz, D. A.; Glatkowski, P. *Appl. Phys. Lett.* **2007**, *90*, 243503.
(5) Cao, Q.; Zhu, Z.; Lemaitre, M. G.; Xia, M.; Shim, M.; Rogers, J. A. *Appl. Phys. Lett.* **2006**, *88*, 113511.
(6) Dan, B.; Irvin, G. C.; Pasquali, M. *ACS Nano* **2009**, *3*, 835−843.
(7) Southard, A.; Sangwan, V.; Cheng, J.; Williams, E. D.; Fuhrer, M. S. *Org. Electron.* **2009**, *10*, 1556−1561.
(8) Tien, H.; Huang, Y.; Yang, S.; Wang, J.; Ma, C. M. *Carbon* **2011**, *49*, 1550−1560.
(9) Bae, S.; Kim, H.; Lee, Y.; Xu, X.; Park, J.; Zheng, Y.; Balakrishnan, J.; Lei, T.; Kim, H. R.; Song, Y. I.; Kim, Y.; Kim, K. S.; Ozyilmaz, B.; Ahn, J.; Hong, B. H.; et al. *Nat. Nanotechnol.* **2010**, *5*, 574−578.
(10) Hecht, D. S.; Hu, L.; Irvin, G. *Adv. Mater.* **2011**, *23*, 1482−1513.
(11) De, S.; Higgins, T. M.; Lyons, P. E.; Doherty, E. M.; Nirmalraj, P. N.; Blau, W. J.; Boland, J. J.; Coleman, J. N. *ACS Nano* **2009**, *3*, 1767−1774.
(12) Lee, J.; Connor, S. T.; Cui, Y.; Peumans, P. *Nano Lett.* **2008**, *8*, 689−692.
(13) Hu, L.; Kim, H. S.; Lee, J.; Peumans, P.; Cui, Y. *ACS Nano* **2010**, *4*, 2955−2963.
(14) Free Copper Price Charts. http://www.metalprices.com/p/CopperFreeChart (accessed December 20, 2013).
(15) Rathmell, A. R.; Bergin, S. M.; Hua, Y.-L.; Li, Z.-Y.; Wiley, B. J. *Adv. Mater.* **2010**, *22*, 3558−3563.
(16) Rathmell, A. R.; Wiley, B. J. *Adv. Mater.* **2011**, *23*, 4798−4803.
(17) Rathmell, A. R.; Nguyen, M.; Chi, M.; Wiley, B. J. *Nano Lett.* **2012**, *12*, 3193−3199.
(18) De, S.; Coleman, J. N. *MRS Bull.* **2011**, *36*, 774−781.
(19) Khaligh, H. H.; Goldthorpe, I. A. *Nanoscale Res. Lett.* **2013**, *8*, 235.
(20) Garnett, E. C.; Cai, W.; Cha, J. J.; Mahmood, F.; Connor, S. T.; Greyson Christoforo, M.; Cui, Y.; McGehee, M. D.; Brongersma, M. L. *Nat. Mater.* **2012**, *11* (241−249), 00070.
(21) Wu, H.; Kong, D.; Ruan, Z.; Hsu, P.-C.; Wang, S.; Yu, Z.; Carney, T. J.; Hu, L.; Fan, S.; Cui, Y. *Nat. Nanotechnol.* **2013**, *8*, 421−425.
(22) Guo, C. F.; Sun, T.; Liu, Q.; Suo, Z.; Ren, Z. *Nat. Commun.* **2014**, DOI: doi:10.1038/ncomms4121.
(23) van de Groep, J.; Spinelli, P.; Polman, A. *Nano Lett.* **2012**, *12*, 3138−3144.
(24) Kang, M.; Guo, L. J. *Adv. Mater.* **2007**, *19*, 1391−1396.
(25) Sotomayor Torres, C.; Zankovych, S.; Seekamp, J.; Kam, A.; Clavijo Cedeño, C.; Hoffmann, T.; Ahopelto, J.; Reuther, F.; Pfeiffer, K.; Bleidiessel, G.; Gruetzner, G.; Maximov, M.; Heidari, B. *Mater. Sci. Eng., C* **2003**, *23* (23−31), 00145.
(26) Kang, M.; Park, H. J.; Ahn, S. H.; Guo, L. J. *Sol. Energy Mater. Sol. Cells* **2010**, *94*, 1179−1184.
(27) Hulteen, J. C. *J. Vac. Sci. Technol. A* **1995**, *13*, 1553.
(28) Haynes, C. L.; Duyne, R. P. V. *J. Phys. Chem. B* **2001**, *105*, 5599−5611.
(29) Wu, H.; Hu, L.; Rowell, M. W.; Kong, D.; Cha, J. J.; McDonough, J. R.; Zhu, J.; Yang, Y.; McGehee, M. D.; Cui, Y. *Nano Lett.* **2010**, *10*, 4242−4248.
(30) Mirri, F.; Ma, A. W. K.; Hsu, T. T.; Behabtu, N.; Eichmann, S. L.; Young, C. C.; Tsentalovich, D. E.; Pasquali, M. *ACS Nano* **2012**, *6*, 9737−9744.
(31) Lide, D. *CRC Handbook of Chemistry and Physics*; CRC Press/Taylor and Francis: Boca Raton, FL, 2010.
(32) Ebbesen, T. W.; Lezec, H. J.; Ghaemi, H. F.; Thio, T.; Wolff, P. A. *Nature* **1998**, *391*, 667−669.
(33) Shin, H.; Catrysse, P. B.; Fan, S. *Phys. Rev. B* **2005**, *72*, 085436.
(34) Fano, U. *Phys. Rev.* **1961**, *124*, 1866−1878.
(35) Ye, X.; Qi, L. *Nano Today* **2011**, *6*, 608−631.
(36) Moon, G. D.; Lee, T. I.; Kim, B.; Chae, G.; Kim, J.; Kim, S.; Myoung, J.-M.; Jeong, U. *ACS Nano* **2011**, *5*, 8600−8612.
(37) Yu, J.; Geng, C.; Zheng, L.; Ma, Z.; Tan, T.; Wang, X.; Yan, Q.; Shen, D. *Langmuir* **2012**, *28*, 12681−12689.
(38) Jeong, S.; Hu, L.; Lee, H. R.; Garnett, E.; Choi, J. W.; Cui, Y. *Nano Lett.* **2010**, *10*, 2989−2994.
(39) Li, J.; Mayer, J. W.; Colgan, E. G. *J. Appl. Phys.* **1991**, *70* (2820−2827), 00172.
(40) Gao, T.; Leu, P. W. *Opt. Express* **2013**, *21*, A419.
(41) Gao, T.; Leu, P. W. *J. Appl. Phys.* **2013**, *114*, 063107.